The Journal of Chemical Physics

Understanding the ordering mechanisms of self-assembled nanostructures of block copolymers during zone annealing

Cite as: J. Chem. Phys. **144**, 114901 (2016); https://doi.org/10.1063/1.4943864
Submitted: 07 December 2015 . Accepted: 28 February 2016 . Published Online: 17 March 2016

Zhinan Cong, Liangshun Zhang, Liquan Wang, and Jiaping Lin

Understanding the ordering mechanisms of self-assembled nanostructures of block copolymers during zone annealing

Zhinan Cong, Liangshun Zhang,[a] Liquan Wang, and Jiaping Lin[a]
Shanghai Key Laboratory of Advanced Polymeric Materials, State Key Laboratory of Bioreactor Engineering, Key Laboratory for Ultrafine Materials of Ministry of Education, School of Materials Science and Engineering, East China University of Science and Technology, Shanghai 200237, China

(Received 7 December 2015; accepted 28 February 2016; published online 17 March 2016)

A theoretical method based on dynamic version of self-consistent field theory is extended to investigate directed self-assembly behaviors of block copolymers subjected to zone annealing. The ordering mechanisms and orientation modulation of microphase-separated nanostructures of block copolymers are discussed in terms of sweep velocity, wall preference, and Flory-Huggins interaction parameter. The simulated results demonstrate that the long-range ordered nanopatterns are achieved by lowering the sweep velocity of zone annealing due to the incorporation of templated ordering of block copolymers. The surface enrichment by one of the two polymer species induces the orientation modulation of defect-free nanostructures through finely tuning the composition of block copolymers and the preference of walls. Additionally, the Flory-Huggins interaction parameters of block copolymers in the distinct regions are main factors to design the zone annealing process for creating the highly ordered nanostructures with single orientation. [http://dx.doi.org/10.1063/1.4943864]

I. INTRODUCTION

Self-assembly of block copolymers into a diversity of periodic nanostructures with feature size of sub-30 nm makes them attractive candidates for fabrications of quantum dots and magnetic storage media as well as integration of next-generation lithography.[1–5] However, the commercial applications of block copolymers to date are still limited due to the difficulties in the spatial control over the long-range ordered nanostructures, which are strongly dependent upon the preparation process. Pursuing the goals of realizing full potential of block copolymers, researchers have prescribed plenty of approaches to produce the defect-free nanostructures, such as the applications of permanent fields (chemical epitaxy,[6,7] topographical epitaxy,[8–14]) and dynamic external fields like shear flow,[15–17] electric fields,[18,19] and thermal gradients.[20–29]

Among the approaches mentioned above, the time- and space-dependent thermal gradients based on the technique of zone annealing or zone refinement are a simple and universally applicable continuous process, which is gaining the importance as a directed self-assembly route for rapidly fabricating the long-range ordered nanostructures of block copolymers.[20,21,27] In the zone annealing method originated from the metallurgy,[30] the materials pass through the thermal gradients so as to restrict the grain growth in narrow space. Zone annealing for the block copolymers can be classified as hot zone annealing (HZA) and cold zone annealing (CZA). In the HZA proposed by Hashimoto and co-workers,[20,21] the block copolymer systems are divided into two regions: α-region with temperature below the order-disorder transition temperature (T_{ODT}) and β-region with temperature above T_{ODT}. The block copolymers in the β-region are in the disordered state while the systems in the α-region undergo the disorder-order transition. As the block copolymer systems slowly pass through the α-region, surface-induced disorder-order transition of block copolymers results in the better long-range ordered nanostructures throughout the entire specimen. It is also found that the relative orientations of nanostructures are influenced by the preferences of walls to different blocks. In contrast to the HZA, the temperatures of block copolymers both in the α- and β-regions of CZA are below T_{ODT}.[27,31–33] The CZA does not disorder the phase-separated domains during the processing. The ordering improvement of self-assembled nanostructures results from the enhanced mobility of polymeric species above the glass transition temperature. It is demonstrated that sweep velocity (corresponding to the position change of thermal gradients per unit time) is an important factor to control the ordering degree of textures. Although the zone annealing method offers a promising opportunity to yield the large-scale well-ordered patterns in short time, the microscopic details of such patterns remain to be definitely elucidated. One particular aspect concerns the ordering mechanisms and the corresponding orientation modulation during the structural evolution of zone-annealed block copolymers.

As a feasible route for validating experimental observations and predicting new phenomena, computer simulations become especially important in promoting better understanding about the structural formation of block copolymers at the microscopic and mesoscopic levels.[34] Nevertheless, the computational studies regarding the ordering kinetics of block copolymers in the presence of zone annealing remain challenging, because the spatiotemporally heterogeneous fields should be incorporated into the kinetic

[a]Electronic addresses: zhangls@ecust.edu.cn and jlin@ecust.edu.cn

model of inhomogeneous polymer fluids. Currently, the computational investigations for the self-assembly behaviors of block copolymers subjected to the zone annealing are very limited.[35–38] For instance, Zhang *et al.* exploited the phenomenological kinetic model to numerically examine the temporal evolution of microphase-separated structures via shifting the phase boundary.[36] Their results suggested that the highly ordered nanostructures are obtained at the low sweep velocity of phase boundary. To explicitly take the conformational entropy of polymer chains into account, Bosse and co-authors utilized an extension of static self-consistent field (SCF) theory to investigate the ordering and orientation phenomena of nanodomains in the presence of thermal gradients.[38] The numerical simulations revealed that the incorporation of spatiotemporally heterogeneous fields has significant effects on the ordering degree and relative orientation of nanostructures. These previous theoretical results enhance our understanding about the equilibrium nanostructures of block copolymers suffered from the dynamic external fields. However, the microscopic kinetics of structural formation of block copolymers subjected to the zone annealing is still in the infancy stage. There remains a need for considerable advancements in terms of the ordering kinetics of self-assembled structures under the various circumstances including the sweep velocity, the copolymer composition, and the wall preference, which facilitate the experimentalists to design the process-directed self-assembly schemes for constructing the device-oriented patterns of block copolymer lithography.

A promising methodology to explore the dynamic behaviors of block copolymers is dynamic extension of SCF theory originally proposed by Fraaije and co-workers.[39] The main idea of the dynamic SCF theory is that the evolution of collective dynamic variables is driven by the chemical potential gradients obtained from the static SCF theory. This method was successfully applied to tackle the issues of structural formation and defect annihilation of block copolymers.[40–44] In the recent works, hybrid dynamic SCF methods coupling with the lattice Boltzmann method and Parrinello-Rahman-Ray technique were developed to examine the hydrodynamic effects on the phase separation of structured fluids and to explore the self-assembly mechanisms of multicomponent polymers, respectively.[45,46] On the basis of these fruitful achievements, the dynamic SCF theory is considered as a powerful tool to probe into the collective kinetics of phase separation of block copolymers, especially for the cases where the chain connectivity is of particular importance.

In this contribution, we aim to extend the dynamic SCF theory to describe the microphase separation of block copolymers subjected to the zone annealing. Such coarse-grained kinetic model is applied to investigate the effects of sweep velocity, copolymer composition, wall preference, and Flory-Huggins interaction parameter on the ordering degree and relative orientation of self-assembled nanostructures. Beyond obtaining the equilibrium features of microphase-separated structures, our model based on the dynamic SCF theory is capable of capturing the dynamic characteristics of structural formation and the orientation modulations of nanostructures, which cannot be resolved by the static SCF simulations and experimental measurements. We expect that the present study may offer fundamental understanding about the control over the long-range ordered nanostructures during the zone annealing and provide some useful guidelines for designing novel materials of block copolymers.

II. MODELING AND METHOD

In the experiments, Hashimoto and co-workers reported a control of macroscopic orientation and ordering degree of block copolymer nanostructures via the hot zone annealing method.[20,21] In this method, the moving temperature gradients are imposed on the block copolymer films placed inside cells with glass surfaces on one end of the films. In order to model such experimental systems and reduce the computational expense, we consider the thin films of block copolymers subjected to the zone annealing along the z direction (see Figure 1), corresponding to the top view of experimental systems in Figure 2 of Ref. 22. The glass surfaces of film specimen are modeled by hard walls. To facilitate the numerical realization of boundary conditions, the walls are imposed on both sides of the films in the z direction, which are marked by red in Figure 1.

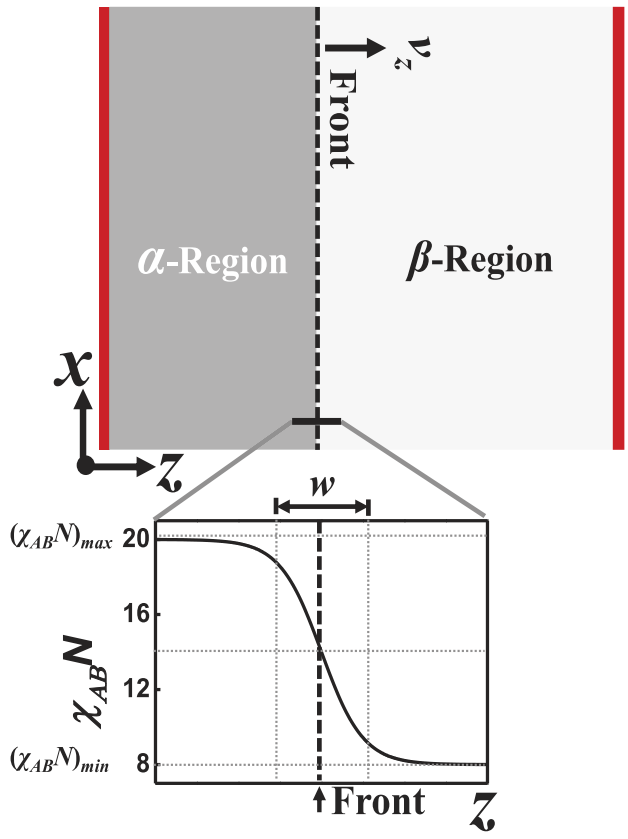

FIG. 1. Schematic diagram of zone annealing model for the block copolymer system. The walls are indicated by the red color. The front marked by the dashed line distinguishes the system into the α-and β-regions, which, respectively, have values of $(\chi_{AB}N)_{max}$ and $(\chi_{AB}N)_{min}$. The front is shifted by a constant velocity v_z along the z direction. Inset is the profile of combined Flory-Huggins interaction parameter $\chi_{AB}N$ at the region of propagating front satisfied the condition $\chi_{AB}(\mathbf{r}, t)N = 0.5\times((\chi_{AB}N)_{max}+(\chi_{AB}N)_{min})$. The definition of zone width w is also schematically illustrated in the inset.

The block copolymer system is modeled by a standard SCF theory of inhomogeneous polymeric fluids. Specifically, the system contains n monodisperse chains of AB block copolymers with length N and volume fraction f_A of A blocks, which are confined between the hard walls. The copolymer chains are specified by the Gaussian threads denoted by function $\mathbf{R}_i(s)$, where s is the curvilinear coordinate of polymer chains and the subscript i labels different chains. A harmonic energy $U = \frac{1}{4R_g^2}\sum_i \int_0^1 ds\left(\frac{d\mathbf{R}_i(s)}{ds}\right)^2$ is used to account for the chain connectivity (R_g is the gyration radius of ideal chain). Interaction energy is modeled by a local contact interaction. For instance, interactions between the A and B species are characterized by the spatiotemporal Flory-Huggins parameter $\chi_{AB}(\mathbf{r},t)$. Deviation of local volume fraction from the average value is represented by the Helfand-type effective energy with coefficient κ_H. Following a standard field-theoretical approach,[47] it is possible to obtain the free energy functional F of the above system in units of thermal energy k_BT written as

$$\frac{F}{n} = -\ln Q + \int d\mathbf{r}\Big\{-\omega_A\varphi_A - \omega_B\varphi_B + \chi_{AB}N\varphi_A\varphi_B + \eta_A N\varphi_A + \eta_B N\varphi_B + \frac{1}{2}\kappa_H(\varphi_A+\varphi_B-1)^2\Big\}, \quad (1)$$

where $\varphi_A(\mathbf{r})$ and $\varphi_B(\mathbf{r})$ are the local volume fractions of A and B blocks, respectively. The quantity Q is the single-chain partition function in the potential fields $\omega_A(\mathbf{r})$ and $\omega_B(\mathbf{r})$ produced by the surrounding chains. Surface fields $\eta_A(\mathbf{r})$ and $\eta_B(\mathbf{r})$ describe the preference of walls for the A and B blocks, respectively. It is assumed that the surface fields with a hyperbolic tangent form decay rapidly away from the walls and the strengths of surface fields at the walls are specified by $\tilde{\eta}_A$ and $\tilde{\eta}_B$. The local volume fractions $\varphi_I(\mathbf{r})$ (I = A and B) are obtained via the formulas

$$\varphi_A(\mathbf{r}) = \frac{1}{Q}\int_0^{f_A} ds\, q(\mathbf{r},s)q^\dagger(\mathbf{r},1-s), \quad (2)$$

$$\varphi_B(\mathbf{r}) = \frac{1}{Q}\int_{f_A}^{1} ds\, q(\mathbf{r},s)q^\dagger(\mathbf{r},1-s). \quad (3)$$

In the expressions, the function $q(\mathbf{r}, s)$ is the end-segment distribution function, representing the probability of finding the sth segment at the coordinate $\mathbf{r}$. The distribution function $q(\mathbf{r}, s)$ is the solution of modified diffusion equation

$$\frac{\partial q(\mathbf{r},s)}{\partial s} = R_g^2\nabla^2 q(\mathbf{r},s) - \omega(\mathbf{r},s)\,q(\mathbf{r},s) \quad (4)$$

subject to initial condition $q(\mathbf{r},0) = 1$ and with $\omega(\mathbf{r}, s) = \omega_A(\mathbf{r})$ for $0 < s < f_A$ and otherwise $\omega(\mathbf{r}, s) = \omega_B(\mathbf{r})$. The function $q^\dagger(\mathbf{r},s)$ is similarly defined.

The kinetics of phase separation in the AB block copolymer system is described by the dynamic extension of SCF theory, which is derived by Fraaije and co-workers.[39] The diffusion behaviors of local volume fractions $\varphi_I(\mathbf{r}, t)$ of I-type blocks are assumed to be driven by the gradients of chemical potentials $\mu_I(\mathbf{r}, t)$. The set of quantities obey the following diffusion equations with the local coupling Onsager coefficients

$$\frac{\partial\varphi_I(\mathbf{r},t)}{\partial t} = L_I\nabla\cdot\varphi_I(\mathbf{r},t)\nabla\mu_I(\mathbf{r},t) + \eta_I, \quad (5)$$

where the terms η_I are the Gaussian thermal noises satisfying the fluctuation-dissipation relationships (e.g., $\langle\eta_I(\mathbf{r},t)\rangle = 0$ and $\langle\eta_I(\mathbf{r},t)\eta_J(\mathbf{r}',t')\rangle = -2L_Ik_BT\delta_{IJ}\nabla\cdot\varphi(\mathbf{r},t)\nabla\delta(\mathbf{r}-\mathbf{r}')\delta(t-t')$). The intrinsic chemical potentials $\mu_I(\mathbf{r},t) \equiv \delta F[\omega_I,\varphi_I]/\delta\varphi_I$ denote the functional derivative of free energy functional $F[\omega_I,\varphi_I]$ with respect to the fields φ_I. L_I are the mobility coefficient of I-type blocks. It should be pointed out that the local coupling model in Eq. (5) neglects the chain connectivity of polymer molecules. It is certain that the Rouse dynamics has a better description of chain dynamics via the intramolecular pair-correlation functions.[48] The difficulty in implementing the Rouse dynamics lies in the computational expense of such functions in the dynamic SCF simulations.

The present model of zone annealing is schematically illustrated in Figure 1. The system consists of the α- and β-regions, which are governed by the combined Flory-Huggins interaction parameter $\chi_{AB}(\mathbf{r}, t)N$ varied in both space and time. The corresponding interaction parameters in the α- and β-regions are represented by the maximum value $(\chi_{AB}N)_{max}$ and the minimum value $(\chi_{AB}N)_{min}$, respectively. It is also assumed that $\chi_{AB}(\mathbf{r}, t)N$ is uniform in the x direction and the connection between $(\chi_{AB}N)_{max}$ and $(\chi_{AB}N)_{min}$ in the z direction has the hyperbolic tangent form (inset of Figure 1(a)). The front distinguishing the α- and β-regions is defined by the condition $\chi_{AB}(\mathbf{r}, t)N = 0.5\times((\chi_{AB}N)_{max} + (\chi_{AB}N)_{min})$. The zone width is represented by the parameter w. The propagation of front in the system is realized as follows: The front is shifted for one lattice space Δz along the z direction in each set of n_t (n = 1, 2,...) steps of time Δt. The sweep velocity of zone annealing is defined as[35]

$$v_z \equiv \frac{\Delta z}{\Delta t\, n_t} = \frac{\Delta\tilde{z}}{\Delta\tilde{t}\, n_t}\tilde{v}, \quad (6)$$

where $\Delta\tilde{z}$ and $\Delta\tilde{t}$ are the dimensionless discrete space and time, respectively. The basic velocity unit is given by $\tilde{v} = R_g/\tau$, which are specified by the basic length unit R_g and time unit τ.

Since the numerical implementations of dynamic SCF theory require a substantial amount of computational cost, all the simulations are performed in the two-dimensional boxes with the periodic and Dirichlet boundary conditions in the x and z directions. Meanwhile, the box size is chosen to be sufficiently large to avoid the simulation artifacts. The operator splitting formula extended by Chantawansti *et al.* is employed to solve the modified diffusion equation (4).[49,50] The discretization of curvilinear coordinate s for the polymer chains is set as 0.01. The evolution equation (5) enforced by the non-flux boundary in the z direction is implemented by the implicit Crank-Nicholson algorithm.[39] The discretization in time is $\Delta\tau = 0.2\tau$, where the time unit is defined as $\tau = \Delta z^2/L_Ik_BT$. The thermal noise terms η_I are discretized by the scheme introduced by van Vlimmeren *et al.* and the amplitude of the Gaussian noises is chosen as $\Omega = 100$.[51] In each time step, the self-consistent determination of the potential fields $\omega_I(\mathbf{r})$ from Eqs. (2)–(4) is done by the Fletcher-Reeves non-linear conjugate gradient method.[52] The iteration

is regarded as convergence when the relative deviation of local volume fractions at each time step becomes less than the error level of 0.01. Further lowering the tolerances has little effects on the final morphologies of nanostructures. Each numerical experiment is repeated 5–8 times with different random seeds.

III. RESULTS AND DISCUSSION

Unless otherwise specified, the simulation boxes presented herein are chosen as 320×320 lattice sites. The size of boxes is set in the range of $56.0R_g \times 56.0R_g$–$68.0R_g \times 68.0R_g$. The interaction parameter between the A and B species in the α-region is fixed at $(\chi_{AB}N)_{max} = 20.0$. The zone width of zone annealing simulations is extremely sharp and is set as $w = 1.5R_g$. In the present work, we apply the model outlined above to investigate the ordering and orientation behaviors of microphase-separated nanostructures under various conditions of zone annealing including the sweep velocity of zone annealing, the preference of walls, and the Flory-Huggins interaction parameter of block copolymers in the β-region. In order to compare with the results of zone annealing simulations, we also perform the reference simulations of homogenous quenching, which start from homogenous states and instantaneously quench into the ordered state in the entire samples.

A. Effects of sweep velocity

We first examine the ordering degree and relative orientation of nanostructures as the fronts move from the left to right of samples. Figure 2 presents the typical final nanostructures of block copolymers with various compositions from the homogenous quenching and zone annealing simulations. The initial configurations of the simulations are the homogenous states and the fronts move with a constant velocity v_z along the z direction. As a special case, $v_z = \infty$ corresponds to the homogenous quenching. Under this circumstance, the spinodal phase separation of block copolymers is triggered by the thermal fluctuations with the random characteristics. This fact results in the formation of polycrystalline structures with several orientations, as depicted in the left panels of Figure 2. It should be mentioned that once the samples are trapped into the polycrystalline states, the ordering degree of nanostructures is hardly improved by the spontaneous ordering due to the large kinetic barriers of structural rearrangement.

To achieve the long-range ordered nanostructures, the zone annealing is introduced to guide the self-assembly of block copolymers.[20,27] Here, the Flory-Huggins interaction parameter in the β-region is set as $(\chi_{AB}N)_{min} = 8.0$ and the walls are assumed to be neutral. The sweep velocity of zone annealing are represented by the basic velocity unit $\tilde{v}$. As the zone annealing process is incorporated into the formation of self-assembled nanodomains, templated ordering exerted by the well-aligned formed nanostructures emerges at the propagating fronts. While the gradients of Flory-Huggins interaction parameter fast sweep the samples, spontaneous phase separation of block copolymers and growth of nanodomains simultaneously occur over a wide swept

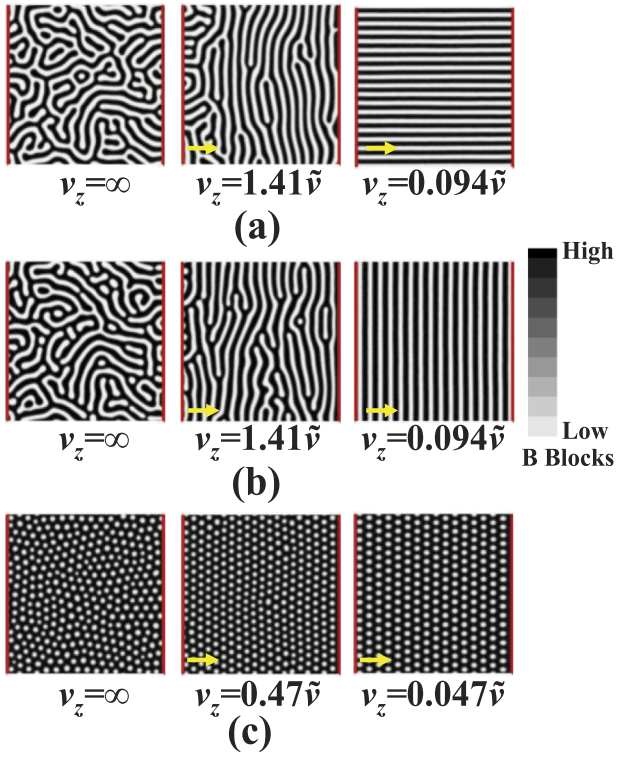

FIG. 2. Representative morphologies of block copolymers with various volume fractions f_A of A-blocks obtained from the homogenous quenching and zone annealing simulations. The volume fractions of A blocks are (a) $f_A = 0.50$, (b) $f_A = 0.45$, and (c) $f_A = 0.30$. The sweep velocities of zone annealing are annotated below the images. $v_z = \infty$ is formally equivalent to the homogenous quenching. The zone annealing corresponds to the cases of infinitesimal sweep velocities. The arrows indicate the moving directions of fronts during the zone annealing process. The color bar indicates the strength of local volume fraction of B blocks.

region of disordered melts. The completion between the spontaneous and templated orderings results in the poorly ordered nanostructures in the entire samples (middle panels of Figure 2). As the fronts are slowly moved, the block copolymers stay in the front regions for a time enough and self-assemble into the templated ordering nanostructures. Via continuously moving the fronts, the templated ordering sequentially occurs from the walls to the other end of simulation cells, and the well-aligned nanostructures are finally achieved (right panels of Figure 2). These results clearly demonstrate that the zone annealing can be utilized to efficiently improve the ordering degree of nanostructures, which is strongly dependent upon the sweep velocities of zone annealing.

Inspecting the right panels of Figure 2 in more details, one can also observe that the orientations of well-ordered nanostructures are correlated with the composition of block copolymers. In the slow mode of zone annealing, the symmetric block copolymers are guided to self-assemble into the well-ordered lamellae perpendicular to the propagating fronts. As the block copolymers become asymmetric (e.g., $f_A = 0.45$), the defect-free lamellae are oriented along the direction of propagating fronts. The further discussion for the orientation modulation of nanostructures will be given below.

To evaluate the generality of self-assembled structures of block copolymers subjected to the zone annealing, we

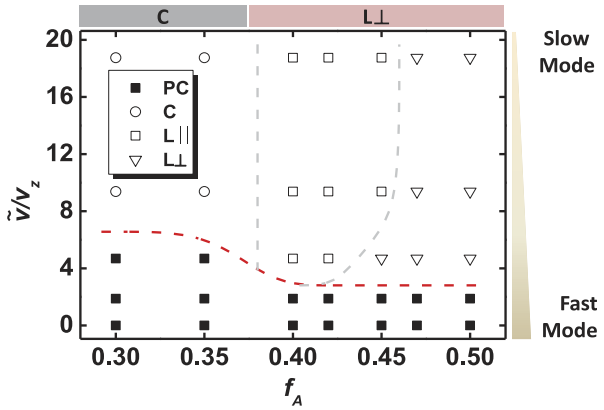

FIG. 3. State diagram of block copolymer nanostructures plotted as functions of volume fraction f_A of A-blocks and reciprocal $\tilde{v}/v_z$ of dimensionless sweep velocity. The notations PC, C, L||, and L⊥ represent the polycrystalline structures, well-ordered cylinders, well-ordered lamellae parallel to the fronts, and well-ordered lamellae perpendicular to the fronts, respectively. Each point in the diagram corresponds to a simulation result, and lines are drawn to identify the boundaries of various nanostructures. The one-dimensional phase diagram on the top of horizontal axis represents the stable regions of cylinders and perpendicular lamellae of block copolymers confined between the neutral walls from the equilibrium SCF calculations.

construct state diagram as functions of the sweep velocity and the copolymer composition, as depicted in Figure 3. Each point in the state diagram corresponds to a simulation result, and the lines are drawn to identify the boundaries of different nanostructures. The state diagram is divided into four characteristic zones: polycrystalline structures (PC), well-ordered lamellae perpendicular to the fronts (L⊥), well-ordered lamellae parallel to the fronts (L||), and well-ordered cylinders (C). In the fast mode of zone annealing simulations, the block copolymers form the poorly ordered structures with several orientations, which are very similar with the cases of homogenous quenching. As the sweep velocities of zone annealing are decreased, the templated ordering of structural formation becomes essential and the block copolymers are guided to self-assemble into the well-ordered nanostructures. In addition, the morphologies and orientations of self-assembled structures are strongly dependent upon the copolymer composition. The transition sequences of lamellae perpendicular to the fronts (L⊥) → lamellae parallel to the fronts (L||) → cylinders (C) are identified as the volume fraction f_A of A-blocks is decreased.

We also utilize the equilibrium SCF simulations in the two-dimensional space to get insight into the self-assembled nanostructures of block copolymers confined between the neutral walls. Via comparing the free energy densities of cylinders, perpendicular and parallel lamellae, the one-dimensional phase diagram of block copolymers is generated. As shown in Figure 3, the structural transition from the cylinders to the perpendicular lamellae occurs at the A-block volume fraction $f_A = 0.364$.[53] In comparison with the stable regions of nanostructures from the zone annealing simulations, one can find one distinct difference that the orientations of self-assembled lamellae are altered by the zone annealing process. As predicted by the equilibrium SCF theory, the perpendicular lamellae are the optimal equilibrium structures in the range of $0.364 < f_A < 0.50$. In the zone annealing simulations, the asymmetric block copolymers probably self-assemble into the parallel lamellae with long-range order. Additionally, the orientations of lamellae are also influenced by the sweep velocity of zone annealing. For example, decreasing the sweep velocity of zone annealing triggers the transition from the optimal perpendicular to parallel orientations in the case of block copolymers at $f_A = 0.45$.

In order to understand the origins of enhanced order and orientation modulation of nanostructures, it is informative to examine the phase separation dynamics of block copolymers in the zone annealing simulations (Figures 4 and 5). Figure 4 presents the morphological evolution of symmetric block copolymers in the zone annealing simulations with various sweep velocities of zone annealing. The propagating fronts are marked by dashed lines. For the sake of clarification, only a portion of the samples are drawn in the high-contrast images. One the right of the dashed lines, the block copolymers do not undergo any phase separation. However, on the left of the dashed lines, the thermodynamic instability is strong enough to drive the microphase separation of block copolymers. When the fronts are fast shifted, the self-assembled lamellae grow rapidly and the orientations of lamellae are random because the spontaneous ordering mainly occurs in the wide swept regions of fronts (Figure 4(a)). As a result, the zone-annealed block copolymers self-assemble into the poorly ordered nanostructures with lots of defects. As depicted in Figure S1 of the supplementary material,[54] such structures

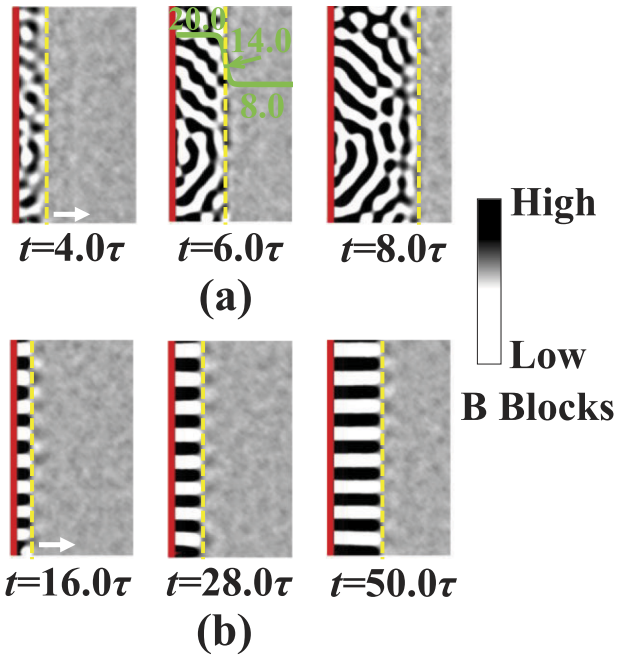

FIG. 4. Morphological evolution of block copolymers in the initial stages of simulations with various sweep velocities of zone annealing (a) $v_z = 1.41\tilde{v}$ and (b) $v_z = 0.094\tilde{v}$. The volume fraction of A blocks is $f_A = 0.5$. Note that only a part of high-contrast images are displayed. The symbol τ represents the time unit of simulations. The dashed lines and the arrows denote the propagating fronts and the moving directions of fronts, respectively. Inset of panel (a) shows the profile of Flory-Huggins interaction parameter along the z directions. The position of dashed line corresponds to the middle of curve. The values of $\chi_{AB}(\mathbf{r}, t)N$ in various regions of zone annealing are shown in the inset.

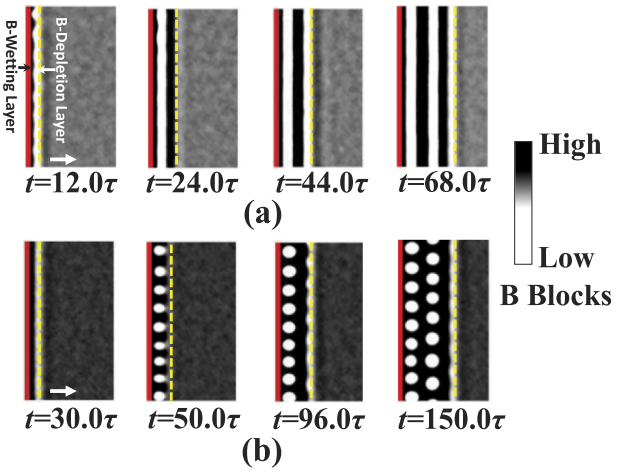

FIG. 5. Morphological evolution of block copolymers with various volume fractions of A-blocks (a) $f_A = 0.45$ and (b) $f_A = 0.30$ in the initial stages of simulations. The sweep velocities of zone annealing are (a) $v_z = 0.094\tilde{v}$ and (b) $v_z = 0.047\tilde{v}$. The representations of lines and arrows are the same as Figure 4.

can further slowly evolve into the highly ordered nanopatterns via the annihilation of defects.

When the fronts are shifted slowly, the microphase separation of block copolymers and the growth of nanostructures occur in the narrow swept regions of fronts, as depicted in Figure 4(b). Under this condition, the existing lamellae in the α-region serve as "chemical templates" to direct the self-assembly of block copolymers in the swept regions. Thus, the perfect order of formed nanostructures is well maintained during the further growth of nanodomains, leading to the defect-free structures of block copolymers.

Figure 5 shows the morphological evolution of block copolymers with various volume fractions of A blocks in the slow mode of zone annealing simulations. In comparison with the symmetric block copolymers, the surface enrichment of certain species takes place in the systems of asymmetric block copolymers despite the neutral walls. As demonstrated in the initial stages of simulations (left panels of Figure 5), the majority B species produce the wetting layers close to the walls and the corresponding depletion layers are produced next to the wetting layers. However, the subsequent pathways for the morphological evolution of depletion layers are strongly dependent upon the copolymer composition. As shown in Figure 5(a), the B-depletion layers of block copolymers with $f_A = 0.45$ are preserved and the flat layers are propagated into the disordered region as the fronts are slowly shifted. While the volume fraction of A blocks is set as $f_A = 0.30$, the B-depletion layers (corresponding to the A-rich layers) are unstable and further transit into the A-rich droplets (Figure 5(b)). An important feature of these droplets is that they have the uniform size and identical position relative to the walls, resulting from the temporal evolution of metastable flat layers. Subsequently, the fresh flat layers are formed with time and the layers further evolve into the A-rich droplets with a relative shift of position. Finally, the well-ordered cylindrical nanostructures of block copolymers are achieved in the process of zone annealing with low sweep velocities.

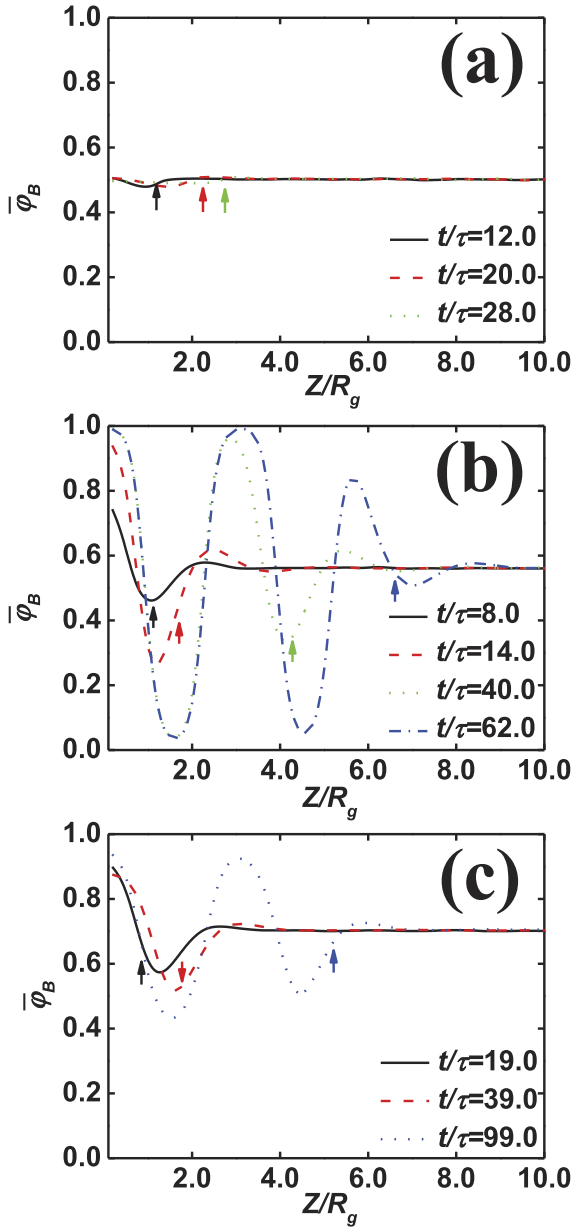

FIG. 6. Profiles of averaged volume fraction $\overline{\varphi}_B$ of B-blocks at different times. The compositions of block copolymers are (a) $f_A = 0.50$, (b) $f_A = 0.45$, and (c) $f_A = 0.30$. The sweep velocities of zone annealing are ((a) and (b)) $v_z = 0.094\tilde{v}$ and (c) $v_z = 0.047\tilde{v}$.

To further clarify the surface enrichment by the B blocks in the initial stages of simulations, we plot the profiles of averaged volume fractions of B blocks along the z direction. The positions of propagating fronts are marked by the arrows. The data of profiles are obtained from averaging the local volume fraction of B blocks given by $\overline{\varphi}_B(z) = \sum_x \varphi_B(x,z)/N_x$, where N_x is the lattice number of simulation boxes in the x direction. Since the symmetric block copolymers form the lamellae perpendicular to the fronts, the averaged volume fractions of B blocks are almost unchanged and the surface enrichment by the polymer species is not identified in the Figure 6(a). As the block copolymers become asymmetric, another scenario is revealed from the profiles of averaged volume fractions, as shown in Figures 6(b) and 6(c). The majority B species are enriched next to the walls and the

enriching process develops gradually as time goes on. In addition, the long enrichment tails of profiles are extended in the β-region of zone annealing. It should be mentioned that the behaviors of surface enrichment were also observed in the binary mixtures of polymers with unequal volume fractions confined between the neutral walls.[37]

To decouple the effects of zone annealing and walls, we carry out the additional simulations of block copolymers subjected to the zone annealing, where the fronts are moved from the bottom to top of boxes. Figure S2 of the supplementary material depicts the morphological evolution of block copolymers at various volume fractions $f_A = 0.50$ and $f_A = 0.45$.[54] It is found that the symmetric block copolymers are guided to self-assemble into the long-range ordered lamellae with orientations perpendicular to the propagating fronts. However, the asymmetric block copolymers form the parallel lamellae. These findings clearly demonstrate that the zone annealing is capable of programming the relative orientations of self-assembled nanostructures of block copolymers under appropriate conditions.

To compare with the available experimental results, we roughly evaluate the relationship between our dimensionless simulation parameters and the dimensional physical values. In particular, we assume the gyration radius of polymer chains as $R_g \sim 10$ nm, and we equate the distance between two lattice sites to be $\Delta z \equiv L_z/N_z = 0.19R_g$ (the box size and total lattice in the z direction are $L_z \sim 60R_g$ and $N_z = 320$, respectively). The basic time unit of Eq. (5) is $\tau = \Delta z^2/L_I k_B T = \Delta z^2/D$, where D is the dimensional diffusion constant. If we take the value of $D \sim 10^{-14}$ m/s^2 in the polymer melts,[55] the time unit corresponds to $\tau = 3.5 \times 10^{-4}$ s and the basic velocity unit $\tilde{v} = R_g/\tau$ has the value of 2.8×10^{-5} m/s. We take the sweep velocity in Figure 2(a) as an example. The velocities $v_z = 1.41\ \tilde{v}$ and $0.094\tilde{v}$ in the simulations correspond to the sweep velocities of 39.5 μm/s and 2.6 μm/s in the realistic experiments, respectively.

There are no direct experimental studies on the self-assembly behaviors of block copolymer thin films in the present of hot zone annealing with temperature above the order-disorder transition temperature (T_{ODT}) in the β-region. Therefore, it is difficult to make a direct comparison between theoretical predictions and experimental observations. However, there are still some existing experimental observations regarding the ordering degree of nanostructures from the zone annealing in the literature to support our simulation results. For example, Hashimoto and co-workers conducted the zone-annealed experiments for the block copolymers with film thickness ~2 mm and low sweep velocity <1 μm/s.[20,23] It is demonstrated that the ordering degree of nanopatterns has a tight relation with the sweep velocity of hot zone annealing. It is noteworthy that Berry *et al.* reported the directed self-assembly of poly(styrene-*block*-methyl methacrylate) thin films via the cold zone annealing with various sweep velocities.[32] Through analyzing the orientation correlation function of nanostructures, it is demonstrated that the defect density of the patterns decreases markedly as the sweep velocity of temperature gradient changes from 100 μm/s to 1 μm/s. In our dynamic SCF simulations, the block copolymers are guided to self-organize into the well-ordered patterns in the cases of slow mode of zone annealing (e.g., $v_z = 2.6$ μm/s or 1.3 μm/s), which is depicted in Figure 2. Although our computer simulations herein carry out for the case of zone annealing with temperature above T_{ODT}, Figures 2 and 3 show an analogous behavior that one can tune the sweep velocity to yield various ordering degree of self-assembled nanostructures.

Beyond obtaining the structural features of block copolymers, the dynamic SCF theory can grasp the microscopic ordering mechanisms of nanostructures via analyzing the snapshots of morphological evolutions. From Figure 4, it is demonstrated that the enhanced order of nanostructures in the slow mode of zone annealing simulations stems from the templated ordering of microphase separation of block copolymers. The orientation modulation of nanostructures results from the surface enrichment by one of the two polymer species (Figure 5). Such microscopic mechanisms of enhanced order and orientation modulation are currently difficult to be deduced from the experimental measurements.

There also exist theoretical investigations to understand the underlying formation mechanisms of well-ordered structures of block copolymers in the presence of zone annealing. For instance, Zhang *et al.* extended the time-dependent Ginzburg-Landau theory to study the microphase separation of diblock copolymers suffering from the moving fronts.[36] It is found that the appearance of highly ordered patterns is preferentially selected by lowering the sweep velocity of zone annealing. Although the phenomenological model of block copolymers is able to reproduce the experimental observations, it ignores the contribution of conformation entropy that is featured in the phase separation of polymers. Additionally, all the theoretical studies do not take the wall preference into account, which play a critical role in controlling the relative orientations of block copolymer nanostructures. Therefore, we advance our research by a step further to investigate the effects of wall preference on the patterns and orientations of block copolymer nanostructures.

B. Effects of wall preference

To investigate the influence of wall preference on the orientations of nanostructures, the zone annealing simulations are performed for the systems with various interaction parameters between the blocks and the walls. For example, the parameter settings $\tilde{\eta}_{AW}N = 1.0$ and $\tilde{\eta}_{BW}N = 0.0$ imply that the walls are repulsive to the A blocks, but are attractive to the B blocks. The sweep velocities of zone annealing are set as $v_z = 0.094\tilde{v}$ to ensure the formation of well-ordered nanostructures.

Figure 7 shows the effects of wall preference on the relative orientations of nanostructures in the slow mode of zone annealing simulations. When the walls are attractive to the majority B blocks, the B-rich flat layers are rapidly developed near the walls in the initial stages of simulations. By collaborating with the process of zone annealing, the B-rich flat layers progressively induce the formation of well-ordered lamellae parallel to the propagating fronts (Figure 7(a)). The enrichment of majority B blocks near the walls is altered if

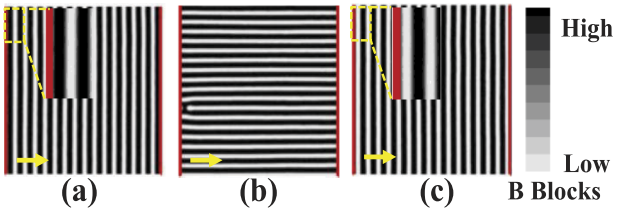

FIG. 7. Representative morphologies of block copolymers with various interaction parameters between the walls and blocks (a) $\tilde{\eta}_{AW}N = 1.0$ and $\tilde{\eta}_{BW}N = 0.0$ (B-attractive walls), (b) $\tilde{\eta}_{AW}N = 0.0$ and $\tilde{\eta}_{BW}N = 0.5$ (weakly B-repulsive walls), and (c) $\tilde{\eta}_{AW}N = 0.0$ and $\tilde{\eta}_{BW}N = 2.0$ (strongly B-repulsive walls). The composition of block copolymers and the sweep velocity of zone annealing are $f_A = 0.45$ and $v_z = 0.094\tilde{v}$, respectively. The arrows indicate the moving directions of fronts in the zone annealing. Insets of images (a) and (c) are the enlarged morphologies enclosed in the dashed boxes.

the affinities of walls are finely tuned. It is interesting that the enrichment of majority B species is compensated as long as the interaction parameters between the B blocks and the walls are increased. As a result, the block copolymers subjected to the zone annealing are guided to self-assemble into the defect-free lamellae perpendicular to the fronts (Figure 7(b)). While the B blocks are strongly repulsive to the walls, the A-rich flat layers are produced next to the walls and the lamellae parallel to the propagating fronts are finally achieved in the slow mode of zone annealing simulations (Figure 7(c)). It should be pointed out that although the block copolymers self-assemble into the defect-free lamellae parallel to the fronts (Figures 7(a) and 7(c)), the local morphologies near the walls display a distinct difference. As shown in insets of Figures 7(a) and 7(c), the block copolymers confined between the B-attractive and B-repulsive walls produce the B-wetting and B-depletion flat layers, respectively.

Figure 8 shows the profiles of averaged volume fractions of B blocks under various conditions of wall preferences in the slow mode of zone annealing simulations. In the cases of strong attractions of walls, it can be seen from Figures 8(a) and 8(c) that the surface enrichment by the certain species is identified due to the specific interactions between the walls and blocks. As the wall affinities are decreased to a suitable value, the driving forces of surface enrichments from the attractions of walls and the asymmetric features of block copolymers are balanced. This can be confirmed if the interaction parameters are set as $\tilde{\eta}_{AW}N = 0.0$ and $\tilde{\eta}_{AW}N = 0.5$. As shown in Figure 8(b), the oscillation of averaged volume fraction profiles becomes weak near the walls in comparison with the cases of strongly attractions of walls. The results suggest that the preference of walls has a large impact on the distributions of polymer compositions in the initial stages of zone annealing.

The preference of walls not only determines the local morphologies of block copolymer nanostructures but also alters the growth rate of wetting layers. If the block copolymers are confined between the neutral walls, the composition profiles are shallow at time $t = 8.0\tau$, as shown in Figure 6(b). Due to the attractions between the majority B blocks and the walls, it is found that the wetting layers grow faster than those in the neutral walls, which are illustrated in Figure 8(a) at time $t = 8.0\tau$. The phenomena manifest the fact that the

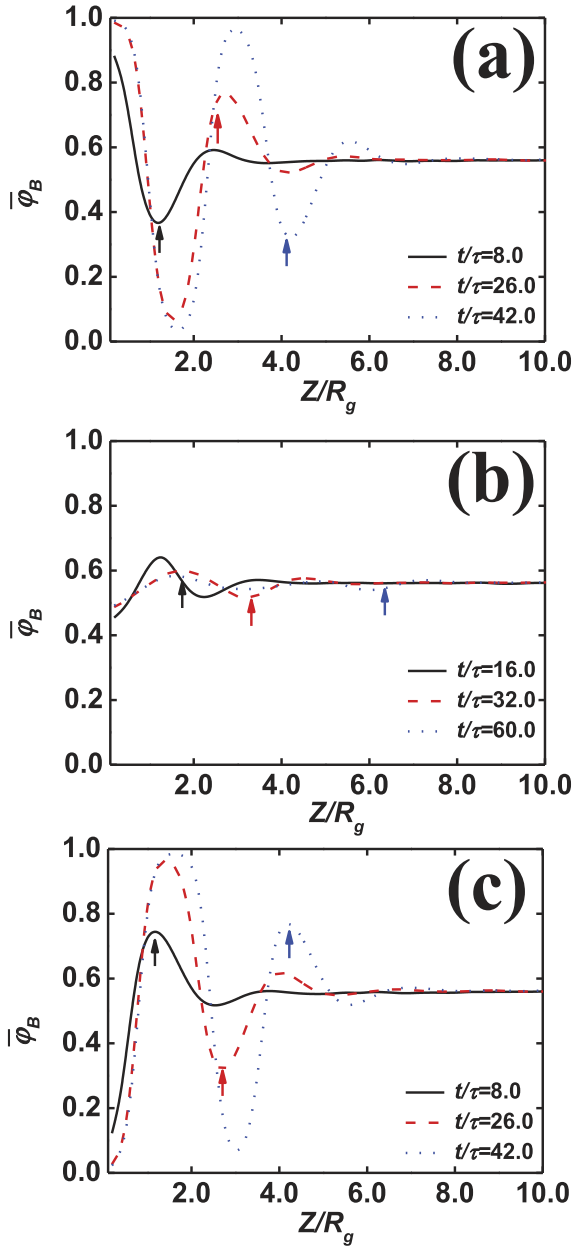

FIG. 8. Profiles of averaged volume fraction $\overline{\varphi}_B$ of B-blocks at different times. The interaction parameters between the walls and blocks are set as (a) $\tilde{\eta}_{AW}N = 1.0$ and $\tilde{\eta}_{BW}N = 0.0$, (b) $\tilde{\eta}_{AW}N = 0.0$ and $\tilde{\eta}_{BW}N = 0.5$, and (c) $\tilde{\eta}_{AW}N = 0.0$ and $\tilde{\eta}_{BW}N = 2.0$. The composition of block copolymers and the sweep velocity of zone annealing are set as $f_A = 0.45$ and $v_z = 0.094\tilde{v}$, respectively.

interactions between the blocks and the walls play a critical role in controlling the growth rate of wetting layers.

As demonstrated above, the short-range attractions between the walls and the blocks only affect the self-assembly behaviors of block copolymers near the walls. This phenomenon results in the formation of highly ordered nanostructures in the vicinity of walls due to the external confinement. With the help of zone annealing process, the surface-induced ordering will propagate into the homogenous phase as the fronts are gradually moved towards the β-region of zone annealing. Eventually, the entire samples are filled by the long-range ordered nanostructures with single orientation.

C. Effects of interaction parameter

In the experiments, one important distinction between the hot and cold zone annealing processes is whether the maximum temperature is above the order-disorder transition temperature (T_{ODT}) or below T_{ODT}. In our current model, we assume that the Flory-Huggins interaction parameter exhibits an inverse dependence on the temperature. To elucidate the effects of maximum temperature on the textures of zone-annealed organic materials, we implement a series of zone annealed simulations with various Flory-Huggins interaction parameters $(\chi_{AB}N)_{min}$ in the β-region.

Figure 9 depicts the morphological evolution of symmetric block copolymers in the presence of zone annealing with various Flory-Huggins interaction parameters $(\chi_{AB}N)_{min}$ = 9.0, 11.0, and 12.0 in the β-region. The sweep velocity and Flory-Huggins interaction parameter in the α-region are set as $v_z = 0.047\tilde{v}$ and $(\chi_{AB}N)_{max} = 20.0$, respectively. It should be mentioned that the order-disorder transition value $(\chi_{AB}N)_{ODT}$ of symmetric block copolymers is 10.5. In the case of $(\chi_{AB}N)_{min} < (\chi_{AB}N)_{ODT}$, it can be seen from Figure 9(a) that the block copolymers in the β-region of zone annealing do not undergo the phase separation. As the fronts are moved along the z direction, templated ordering occurs sequentially from the walls towards the interior of simulation boxes, and finally the well-ordered nanostructures are formed in the slow mode of zone annealing (Figure 9(a)). As the $(\chi_{AB}N)_{min}$ is larger than $(\chi_{AB}N)_{ODT}$ = 10.5, the feature of microphase separation can be also identified in the β-region, which is shown in the Figures 9(b) and 9(c). However, the contrast between the two phases in the β-region is shallow, indicating that the extent of phase separation is very low when $(\chi_{AB}N)_{min}$ = 11.0 (Figure 9(b)). Under this circumstance, the template ordering is able to guide the block copolymers to form the highly ordered structures via the local rearrangement of formed domains. While the $(\chi_{AB}N)_{min}$ is increased to 12.0, the microphase separation of block copolymers takes place in the entire simulation boxes and the irregularly shaped domains fill the α- and β-regions of films. The slow movement of fronts is not strong enough to annihilate the defects within the time scale of our simulations. As a result, the polycrystalline configurations with several lamellar grains are produced in the block copolymer films suffered from the zone annealing with higher value of $(\chi_{AB}N)_{min}$ (Figure 9(c)). From above observations, one can find that the Flory-Huggins interaction parameter $(\chi_{AB}N)_{min}$ of zone annealing is a significant factor to control the ordering degree of self-assembled nanostructures.

To systemically capture the self-assembly behaviors of zone-annealed block copolymers, we construct state diagram in terms of the Flory-Huggins interaction parameter $(\chi_{AB}N)_{min}$ and the reciprocal $\tilde{v}/v_z$ of sweep velocity, as depicted in Figure 10. It should be noted that the vertical axis has a logarithmic scale. The line is drawn to identify the critical sweep velocity $(v_z/\tilde{v})^*$, which corresponds to the highest sweep velocity of zone annealing leading to the formation of well-ordered perpendicular lamellae. Based on how the critical sweep velocity of zone annealing is affected by the Flory-Huggins interaction parameter, the diagram is divided into three characteristic regions, which are marked by the Roman numbers. In the characteristic region I ($(\chi_{AB}N)_{min} \le 9.0$), the critical sweep velocity $(v_z/\tilde{v})^*$ is almost equal, since the block copolymers in the β-region are in the homogenous states. In the characteristic region II ($10.0 \le (\chi_{AB}N)_{min} < 13.0$), an increase of Flory-Huggins interaction parameter leads to the occurrence of microphase separation of block copolymers in the β-region of zone annealing. To achieve the defect-free patterns, the critical sweep velocity $(v_z/\tilde{v})^*$ is decreased exponentially (correspond to the increase of reciprocal

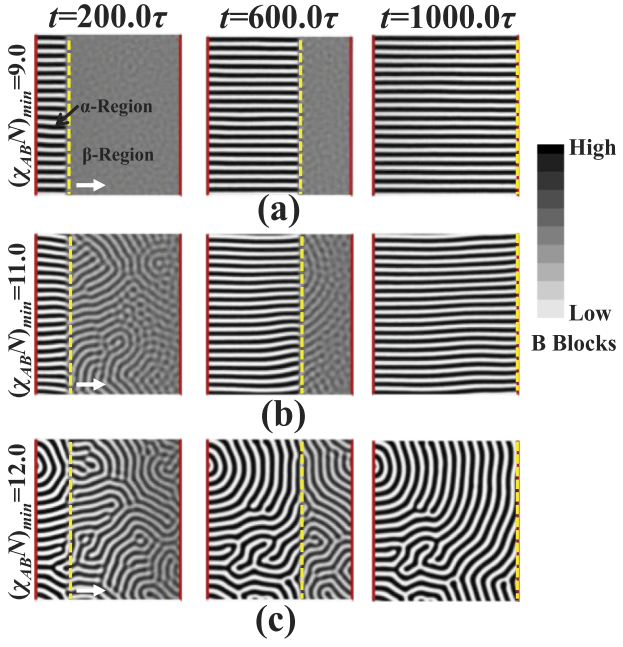

FIG. 9. Morphological evolution of block copolymers at various Flory-Huggins interaction parameters in the β-region of zone annealing (a) $(\chi_{AB}N)_{min}$ = 9.0, (b) $(\chi_{AB}N)_{min}$ = 11.0, and (c) $(\chi_{AB}N)_{min}$ = 12.0. The left, middle, and right panels correspond to the times $t = 200.0\tau$, 600.0τ, and 1000.0τ, respectively. The sweep velocity and Flory-Huggins interaction parameter in the α-region are $v_z = 0.047\tilde{v}$ and $(\chi_{AB}N)_{max} = 20.0$, respectively. The dashed lines and the arrows represent the propagating fronts and the moving directions of fronts, respectively.

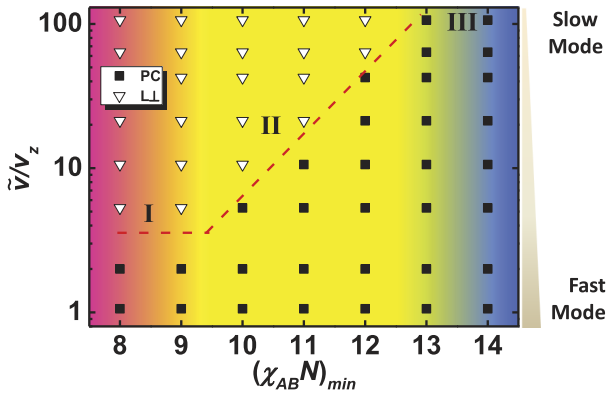

FIG. 10. State diagram of block copolymer nanostructures plotted as functions of reciprocal $\tilde{v}/v_z$ of dimensionless sweep velocity and Flory-Huggins interaction parameter $(\chi_{AB}N)_{min}$ in the β-region of zone annealing. Note that the vertical axis has a logarithmic scale. The notations PC and L$\perp$ represent the polycrystalline structures and well-ordered lamellae perpendicular to the fronts, respectively. The red dashed line is drawn to identify the critical sweep velocity $(v_z/\tilde{v})^*$, which denotes the highest sweep velocity of zone annealing leading to the formation of well-ordered nanostructures. The background colors indicate the different regions marked by Roman numbers.

of sweep velocity). Beyond the Flory-Huggins interaction parameter $(\chi_{AB}N)_{min} > 13.0$, the large-cell simulations for the block copolymers usually produce the poorly ordered nanostructures. The above observations suggest that the formation of well-ordered nanostructures of zone-annealed block copolymers is strongly dependent upon the sweep velocity and the Flory-Huggins interaction parameter in the β-regions, which are main factors to design the zone annealing process for creating the organic materials with single orientation.

We would like to emphasize that there are other physical models to understand the directed self-assembly behaviors of block copolymers subjected to the cold zone annealing with the temperature below T_{ODT} or $(\chi_{AB}N)_{min} > (\chi_{AB}N)_{ODT}$. Inspired by the zone annealing for the glassy block copolymers under the conditions where the entire samples are in the phase-separated state, Bosse *et al.* introduced the spatiotemporally heterogeneous mobility to model the intrinsic time- and space-dependent thermal fields of zone annealing for the glassy polymer fluids.[38] The computer simulations demonstrated that the sweep velocity of mobility gradient plays a critical role in controlling the ordering degree of microphase-separated nanostructures of block copolymers. Although our simulations can reproduce the general trends of ordering degree in terms of the sweep velocity of zone annealing (see Figures 2 and 3), the kinetic model of SCF theory neglects important aspects of glassy characteristic of polymer molecules in the realistic experiments. Therefore, the current zone annealing model based on the dynamic SCF theory cannot be extended to describe the systems of glassy polymers due to the instantaneous response of monomers to the driving fields. Recent developments in phase-field crystal (PFC) modeling make it possible to tackle the issues of glass transition kinetics of simple fluids.[56] For instance, Berry and Grant utilized the PFC modeling of binary mixture to examine the dynamics of glass-forming fluids across a large range of time scales.[57] The motion equations describing two or more time scales generate two-step relaxation functions in the supercooled liquids, which are generally in line with the basic features predicted by the mode-coupling theory of glass formation. Combining such motion equations and SCF theory provides a feasible scheme for describing the glassy dynamics of polymer fluids in the presence of cold zone annealing.

It should be mentioned that the zone width in the current simulations is extremely narrow, in comparison with the typical width (~40 μm) of thermal gradients reported in experiments.[29] To elucidate the effects of zone width on the self-assembled nanostructures, we implement a series of zone annealing simulations with various zone widths at the sweep velocity $v_z = 0.19\tilde{v}$. Figure S3 of supplementary material displays the typical morphologies of block copolymers under various zone widths.[54] The block copolymers self-assemble into the single orientation of lamellae under the condition of sharp zone annealing. As the zone width is increased, the ordering of nanodomains occurs in the large phase-separated space, resulting in the poorly ordered nanostructures despite the slow mode of zone annealing.

As stated above, the broad zone widths cause the prediction alternations of dynamic SCF theory. In other words, the state diagram of Figure 3 may experience some degree of shifts when the zone widths become broader. Yet the computational findings under the condition of sharp zone widths provide useful guidelines for rationally designing the zone annealing process of block copolymer systems that include the broad gradient of Flory-Huggins interaction parameter (e.g., the long-rang ordered nanostructures can be achieved by further lowering the sweep velocity). For example, the block copolymers subjected to the zone annealing with the sweep velocity $v_z = 0.19\tilde{v}$ and zone width $w = 28.1R_g$ form the multi-orientation nanopatterns (Figure S3(d) of the supplementary material).[54] As the sweep velocity is chosen as $v_z = 0.094\tilde{v}$, the organic materials are guided to produce the single-orientation textures. It should be mentioned that the computational intensity of zone annealing simulations at the very low sweep velocity is enlarged greatly. Currently, the acceleration techniques via graphics-processing-units are addressing the challenges of large-cell and long-time simulations in three dimensions.[58] Detailed studies based on such techniques will be devoted to thoroughly elucidating the generality of long-range ordered nanostructures of zone-annealed block copolymers in terms of the sweep velocity and zone width.

IV. CONCLUSIONS

In summary, we extend the dynamic SCF theory to model the directed self-assembly of block copolymers subjected to the zone annealing. Our simulated results demonstrate that the ordering and orientation of microphase-separated nanostructures have a tight relation with the sweep velocity of zone annealing. Beyond obtaining the structural features, the numerical simulations grasp the microscopic ordering mechanisms of block copolymer nanostructures in the presence of zone annealing. The enhanced order and orientation modulation of nanostructures result from the templated ordering and the surface enrichment by the certain species in the microphase separation of block copolymers, respectively. The simulated results also prove that the short-range interactions between the walls and blocks are able to mediate the relative orientations of long-range ordered structures of block copolymers during the zone annealing. In addition, the critical sweep velocities of zone annealing that induced the formation of well-ordered nanostructures are exponentially lowered as the block copolymers in the β-region are in the microphase-separated states.

ACKNOWLEDGMENTS

This work was supported by the National Natural Science Foundation of China (Nos. 51203049, 21574040, and 21234002) and the Fundamental Research Funds for the Central Universities. Support from 111 Project (No. B14018) is also appreciated. The authors are also grateful to the anonymous reviewers for their comments and suggestions, which result in an improvement of the paper.

[1]J. Chai and J. M. Buriak, ACS Nano **2**, 489 (2008).
[2]D. Zschech, D. H. Kim, A. P. Milenin, R. Scholz, R. Hillebrand, C. J. Hawker, T. P. Russell, M. Steinhart, and U. Gösele, Nano Lett. **7**, 1516 (2007).

[3]K. Naito, H. Hieda, M. Sakurai, Y. Kamata, and K. Asakawa, IEEE Trans. Magn. **38**, 1949 (2002).
[4]K. Banerjee, S. J. Souri, P. Kapur, and K. C. Saraswat, Proc. IEEE **89**, 602 (2001).
[5]H.-C. Kim, S.-M. Park, and W. D. Hinsberg, Chem. Rev. **110**, 146 (2010).
[6]M. P. Stoykovich, M. Müller, S. O. Kim, H. H. Solak, E. W. Edwards, J. J. de Pablo, and P. F. Nealey, Science **308**, 1442 (2005).
[7]R. Ruiz, H. Kang, F. A. Detcheverry, E. Dobisz, D. S. Kercher, T. R. Albrecht, J. J. de Pablo, and P. F. Nealey, Science **321**, 936 (2008).
[8]R. A. Segalman, A. Hexemer, and E. J. Kramer, Macromolecules **36**, 6831 (2003).
[9]D. Sundrani, S. B. Darling, and S. J. Sibener, Nano Lett. **4**, 273 (2004).
[10]J. Chai, D. Wang, X. Fan, and J. M. Buriak, Nat. Nanotechnol. **2**, 500 (2007).
[11]M. R. Hammond, E. Cochran, G. H. Fredrickson, and E. J. Kramer, Macromolecules **38**, 6575 (2005).
[12]R. Ruiz, N. Ruiz, Y. Zhang, R. L. Sandstrom, and C. T. Black, Adv. Mater. **19**, 2157 (2007).
[13]I. Bita, J. K. W. Yang, Y. S. Jung, C. A. Ross, E. L. Thomas, and K. K. Berggren, Science **321**, 939 (2008).
[14]X. He, Z. Zou, D. Kan, and H. Liang, J. Chem. Phys. **142**, 101912 (2015).
[15]Z.-R. Chen, J. A. Kornfield, S. D. Smith, J. T. Grothaus, and M. M. Satkowski, Science **277**, 1248 (1997).
[16]Z. Qiang, L. Zhang, G. E. Stein, K. A. Cavicchi, and B. D. Vogt, Macromolecules **47**, 1109 (2014).
[17]S. Y. Kim, A. Nunns, J. Gwyther, R. L. Davis, I. Manners, P. M. Chaikin, and R. A. Register, Nano Lett. **14**, 5698 (2014).
[18]K. Amundson, E. Helfand, D. D. Davis, X. Quan, S. S. Patel, and S. D. Smith, Macromolecules **24**, 6546 (1991).
[19]C. Liedel, C. W. Pester, M. Ruppel, V. S. Urban, and A. Böker, Macromol. Chem. Phys. **213**, 259 (2012).
[20]T. Hashimoto, J. Bodycomb, Y. Funaki, and K. Kimishima, Macromolecules **32**, 952 (1999).
[21]J. Bodycomb, Y. Funaki, K. Kimishima, and T. Hashimoto, Macromolecules **32**, 2075 (1999).
[22]K. Mita, H. Tanaka, K. Saijo, M. Takenaka, and T. Hashimoto, Macromolecules **40**, 5923 (2007).
[23]K. Mita, H. Tanaka, K. Saijo, M. Takenaka, and T. Hashimoto, Macromolecules **41**, 6780 (2008).
[24]K. Mita, H. Tanaka, K. Saijo, M. Takenaka, and T. Hashimoto, Macromolecules **41**, 6787 (2008).
[25]K. Mita, M. Takenaka, H. Hasegawa, and T. Hashimoto, Macromolecules **41**, 8789 (2008).
[26]D. E. Angelescu, J. H. Waller, D. H. Adamson, R. A. Register, and P. M. Chaikin, Adv. Mater. **19**, 2687 (2007).
[27]B. C. Berry, A. W. Bosse, J. F. Douglas, R. L. Jones, and A. Karim, Nano Lett. **7**, 2789 (2007).
[28]G. Singh, K. G. Yager, B. Berry, H.-C. Kim, and A. Karim, ACS Nano **6**, 10335 (2012).
[29]G. Singh, K. G. Yager, D. M. Smilgies, M. M. Kulkarni, D. G. Bucknall, and A. T. Karim, Macromolecules **45**, 7107 (2012).
[30]W. G. Pfann, *Zone Melting*, 2nd ed. (John Wiley & Sons, 1966).
[31]K. G. Yager, N. J. Fredin, X. Zhang, B. C. Berry, A. Karim, and R. L. Jones, Soft Matter **6**, 92 (2010).
[32]B. C. Berry, G. Singh, H.-C. Kim, and A. Karim, ACS Macro Lett. **2**, 346 (2013).
[33]G. Singh, S. Batra, R. Zhang, H. Yuan, K. G. Yager, M. Cakmak, B. Berry, and A. Karim, ACS Nano **7**, 5291 (2013).
[34]D. Frenkel and B. Smit, *Understanding Molecular Simulation: From Algorithms to Applications*, 2nd ed. (Academic Press, 2007).
[35]H. Furukawa, Physica A **180**, 128 (1992).
[36]H. Zhang, J. Zhang, Y. Yang, and X. Zhou, J. Chem. Phys. **106**, 784 (1997).
[37]B. Liu, H. D. Zhang, and Y. L. Yang, J. Chem. Phys. **113**, 719 (2000).
[38]A. W. Bosse, J. F. Douglas, B. C. Berry, R. L. Jones, and A. Karim, Phys. Rev. Lett. **99**, 216101 (2007).
[39]J. G. E. M. Fraaije, B. A. C. van Vlimmeren, N. M. Maurits, M. Postma, O. A. Evers, C. Hoffmann, P. Altevogt, and G. Goldbeck-Wood, J. Chem. Phys. **106**, 4260 (1997).
[40]C. Yeung and A.-C. Shi, Macromolecules **32**, 3637 (1999).
[41]E. Reister, M. Müller, and K. Binder, Phys. Rev. E **64**, 041804 (2001).
[42]H. Morita, T. Kawakatsu, M. Doi, D. Yamaguchi, M. Takenaka, and T. Hashimoto, Macromolecules **35**, 7473 (2002).
[43]N. Xie, W. Li, H. Zhang, F. Qiu, and A.-C. Shi, J. Chem. Phys. **139**, 194903 (2013).
[44]Y. Xu, N. Xie, W. Li, F. Qiu, and A.-C. Shi, J. Chem. Phys. **137**, 194905 (2012).
[45]L. Zhang, A. Sevink, and F. Schmid, Macromolecules **44**, 9434 (2011).
[46]X. Cao, L. Zhang, L. Wang, and J. Lin, Soft Matter **10**, 5916 (2014).
[47]G. H. Fredrickson, *The Equilibrium Theory of Inhomogeneous Polymers* (Oxford University Press, 2006).
[48]M. Müller and F. Schmid, Adv. Polym. Sci. **185**, 1 (2005).
[49]G. Tzeremes, K. Ø. Rasmussen, T. Lookman, and A. Saxena, Phys. Rev. E **65**, 041806 (2002).
[50]T. L. Chantawansri, S.-M. Hur, C. J. Garcia-Cervera, H. D. Ceniceros, and G. H. Fredrickson, J. Chem. Phys. **134**, 244905 (2011).
[51]B. A. C. van Vlimmeren and J. G. E. M. Fraaije, Comput. Phys. Commun. **99**, 21 (1996).
[52]W. H. Press, S. Teukolsky, W. Vetterling, and B. P. Flannery, *Numerical Recipes in Fortran: The Art of Scientific Computing* (Cornell University Press, 1992).
[53]M. W. Matsen, J. Chem. Phys. **106**, 7781 (1997).
[54]See supplementary material at http://dx.doi.org/10.1063/1.4943864 for the morphological evolution of block copolymers as well as the effects of zone widths.
[55]O. Kuksenok, R. D. M. Travasso, and A. C. Balazs, Phys. Rev. E **74**, 011502 (2006).
[56]N. Provatas and K. Elder, *Phase-Field Methods in Materials Science and Engineering* (Wiley-VCH, 2010).
[57]J. Berry and M. Grant, Phys. Rev. E **89**, 062303 (2014).
[58]L. Zhang, L. Wang, and J. Lin, ACS Macro Lett. **3**, 712 (2014).